J Electroceram (2012) 28:261–267
DOI 10.1007/s10832-012-9725-4

Dielectric and magnetic properties of sol–gel derived mullite-iron nanocomposite

Debasis Roy · Biswajoy Bagchi · Sukhen Das · Papiya Nandy

Received: 23 August 2011 / Accepted: 2 April 2012 / Published online: 26 April 2012

Abstract Synthesis of highly crystallized mullite has been achieved at a temperature of 1000°C by sol–gel technique in presence of iron ions of different concentrations. XRD, FTIR spectroscopy, FESEM, LCR meter and HyMDC, Hysteresis measurement instrument, characterized samples. Mullite formation was found to depend on the concentration of the ions. The dielectric properties (dielectric constant, tangent loss and a.c. conductivity) of the composites have been measured, their variation with increasing frequency and concentration of the doped metal was investigated, and magnetic behavior was observed from the hysteresis loops. All the experimentations were performed at the room temperature. The composite showed a minimum dielectric constant of 3.26 at 0.002(M) concentration of iron at 1.5 MHz and the magnetic properties of nanocomposites suggest that the iron nanoparticles show hysteresis loop in 0.10 M, 0.15 M and 0.20 M , hence acts like typical paramagnetic materials as is the case for other iron-doped ferrisilicates.

Keywords Mullite · Sol–gel · XRD · Dielectric properties · Magnetic property

1 Introduction

Microelectronics industry is continuously trying to develop processes that are more advanced and which lead to forecasting transistor density, chip complexity, and operating speed or frequency for future technological developments. The main challenge is to carry electric power and to distribute the clock signals that control the timing and synchronize the operation. This challenge extends beyond the material properties and technology and also involves system architecture. The propagation velocity of electromagnetic waves will become increasingly important due to their unyielding constraints on interconnect delay. Interconnect technology is the main factor for signal delay. The impact of delay will undoubtedly increase as we move into the nanometer region. Now the materials with low-*k* dielectrics will be suitable for lowering signal delay. Hence, they can be used in high-speed circuits as well as in high package density substrate [1–4].

Mullite based composites have been increasingly gaining importance for high frequency circuit packaging and electronic substrate application due to their low dielectric constant (~6) and low thermal expansion coefficient. Earlier, alumina was used as substrate but the comparatively high dielectric constant (~9) increases the signal transmission delay time (t_d).The dielectric constant of the medium determines the speed of the signal passing through it. The signal transmission delay time (t_d) is given by $t_d=(\epsilon_r*s)1/2/c$, where, ϵ_r is the dielectric constant of the medium, s is the signal path length and c is the velocity of light. For high performance circuits 't_d' should be as low as possible. Hence mullite with its low dielectric constant is most suitable for such application [2–7].

Nanocomposite materials containing magnetic particles are very interesting in many applications since they exhibit new exciting electronic, magnetic and optical properties.

Several reports have been published dealing with synthesis of mullite composites in presence of various 'mineralizers'

D. Roy · B. Bagchi · S. Das (✉) · P. Nandy
Physics Department, Jadavpur University,
Kolkata 700 032, India
e-mail: debasis35@yahoo.co.in

which improve the mechano-chemical properties (densification, porosity, mechanical strength, sintering temperature, surface area etc.), and also there are some recent publications related to the dielectric properties and magnetic properties of these modified mullite composites [8–14].

We have studied the dielectric constant, loss tangent, a.c. conductivity and magnetization of the mullite composites doped with varying concentrations of iron ions with different frequencies at room temperature. The results indicate that the sample G_1 is having lowest dielectric constants 3.26 at frequency 1.5 Mhz. Iron based composites can be used in high-speed circuits and as high package density substrate [4].

2 Experimental

2.1 Sample materials

Chemicals used in the preparation of mullite precursor gels are Aluminium nitrate nonahydrate($Al(NO_3)_3.9H_2O$) extra pure(MERCK, India), Aluminium isopropoxide ($Al(-O\text{-}i\text{-}Pr)_3$) puriss (Spectrochem Pvt.Ltd., India.), Tetra ethyl orthosilicate ($Si(OC_2H_5)_4$),(MERCK, Germany), Iron Nitrate($Fe(NO_3)_3{\cdot}9H_2O$) (MERCK Specialities Pvt. Ltd., India).

2.2 Sample preparation and characterization

Mullite precursor gel powder was synthesized by dissolving stoichiometric amounts of $Al(-O\text{-}i\text{-}Pr)_3$ (puriss, Spectrochem Pvt. Ltd., Mumbai, India)and TEOS (Merck,Germany) in 0.5 (M) solution of $Al(NO_3)_3.9H_2O$ (extra pure, Merck, Worli, Mumbai, India) [15, 16]. Molar ratio of $Al(-O\text{-}i\text{-}Pr)_3/Al(NO_3)_3.9H_2O$ was kept at 7:2 in order to form spinnable sols. The mole ratio of Al/Si was 3:1 [17] and the pH of the solution was measured to be 5.

The iron nitrate salts were added to the original solution in the ratio Al: Si: x, where x is the concentration of the metal salt in molarity. The iron salts were added such that in the final solution x=0.002 M, 0.02 M, 0.1 M, 0.15 M & 0.2 M [13, 14]. The sol's Gelation took place after vigorous stirring for 3 hours and the sol was maintained overnight at 60°C. Finally, the gel was dried at 110°C and ground to a free flowing powder .The samples were then pelletized (426 $mm^2 \times 2.7$ mm) and sintered at 1000°C for 2 hrs in a muffle furnace under air atmosphere (heating rate 10°C/min.) [18–21]

Finally cylindrical pellets of 1 mm thickness were prepared by pressing powder to 64 MPa in a 10 mm diameter stainless steel die using hydraulic press. The designation of the samples with their composition is given below (see Table 1).

Table 1 Samples with their compositions sintered at 1000°C containing increasing concentration of iron

Samples at 1000°C	Composition	Conc. of iron ions in molarity
G_0	Mullite precursor gel	0.000 M
G_1	Mullite precursor gel	0.002 M
G_2	Mullite precursor gel	0.020 M
G_3	Mullite precursor gel	0.100 M
G_4	Mullite precursor gel	0.150 M
G_5	Mullite precursor gel	0.200 M

2.3 Instruments used

2.3.1 Density determination

Density of the samples was determined by using displacement method. According to Archimedes principle the density of the sample ρ=m / V, where m is the mass of the sample and V is the volume was determined by the displacement method [22]

2.3.2 X-ray technique

The crystalline phases developed in the samples sintered at 1000°C were analyzed by X-ray Powder Diffractometer (model-D8, Bruker AXS, Wisconsin, USA.) using Cu Kα radiation- 1.5418 Å and operating at 40 KV with a scan speed of 1 sec/step.

2.3.3 FTIR analysis

The characteristic stretching and bending modes of vibration of chemical bonds of a sample can be effectively evaluated by spectroscopic methods. 1 % sample was mixed with spectroscopy grade KBr, pelletized to form disc and analyzed by FTIR spectroscopy (FTIR-8400 S, Shimadzu).

2.3.4 Dielectric measurements

The AC parameters such as capacitance (c) and dissipation factor (tan δ) of the samples were measured in the frequency range 500 Hz to 1.5 MHz using LCR meter (HP Model 4274 A, Hewlett-Packard, USA). The variation of dielectric constant and loss tangent were studied by recording these parameters using sample pellets of uniform thickness at ten different frequencies from 500 Hz to 1.5 MHz.

2.3.5 FESEM

Morphology of the sintered gels were observed by Field Emission Scanning Electron Microscope (FESEM) (JSM 6700F, JEOL Ltd. Tokyo, Japan). Samples were etched with

25 % HF solution. About 2 mg of each sample was dispersed in ethanol and a single drop was placed on copper grid for sample preparation.

2.3.6 Magnetic measurements

The magnetic measurement of the nanocomposite was carried out by HyMDC, Hysteresis measurement instrument (Metis Instruments and Equipment NV, Leuven Belgium). The nanocomposite samples are put into the sample chamber having cross section 0.05 mm ^{2} and the density of the sample is supplied for each sample G_0 (1830 kg /m^3) to G_5(3500 kg /m ^{3}). The frequency is kept at 5 Hz through out the experimentation and the sensitivity is adjusted accordingly.

2.4 Results and discussion

2.4.1 Density analysis

The density of the lowest 0.002 M (G_1) and highest 0.2 M (G_5) concentration of doped iron composites were determined. It has been observed that as doping concentration increases density also increases. From X-ray Diffraction and FESEM, it can be seen that mullite content increases with doping concentration. The density of the composite also increases with the increasing concentration, which may be due to the increased mullite content and metal concentration of the samples.

2.4.2 X-ray diffraction analysis

From the x-ray diffractograms, it can be seen that the undoped sample shows considerable mullite phase at 1000°C, while for the doped samples, also prominent mullite peaks were obtained & they are changing with the concentrations. Mullite phase increases with increasing concentration of iron ions uptoG_3 (see Fig. 1).Increasing the concentration of iron ion has an important role on mullite growth as can be seen from the relative peak intensities with the increase of iron concentration. The analysis indicates that iron ion positively influenced the mullitization process. However, the efficiency of iron ion is lost as the concentration increases beyond G_3 [13, 14]. Interaction of the iron ions with the alumina and silica component of the gel is responsible for the incorporation of accelerated transformation to mullite phase [13, 14, 19].

A glassy phase has been observed during mullite formation according to the results of x-ray analysis and it increases (glass phase is indicated by) as the concentration of the doped iron increases. Form G_2 to G_5 samples, apart from mullite other reflections were observed which may be due to the formation of metal aluminates and silicates (Fig. 1).

2.4.3 FTIR analysis

By spectroscopic method, the characteristic stretching and bending modes of vibration of chemical bonds of a sample can be effectively evaluated. 1 % sample was mixed with spectroscopy grade KBr, pelletized to form disc and analyzed by FTIR (FTIR-8400 S, Shimadzu). Mullite gives characteristic bands at wave numbers around 560, 730, 840, 1060, 1130 and 1170 cm^{-1}[14]. Figure 2 shows the FTIR spectra of the Iron doped sintered gels. All the characteristic bands of mullite- 561 (AlO_6), 741(AlO_4), 837 (AlO_4), 900(AlO_4 stretching mode) and 1141 cm^{-1} (Si–O stretching mode) appear in all the doped samples. There is no band around 1380 cm^{-1} or 1630 cm^{-1}, indicating removal of volatile components. Absence of band around 1170 cm^{-1} indicates primarily a tetragonal geometry for mullite [23–25].

2.4.4 Dielectric measurements

The dielectric constant (k) or relative permittivity (ϵ_r) of each sample was calculated from the capacitance using the formula

$$\epsilon_r = (C \times d) / A \epsilon_o ,$$

Where, C is the capacitance of the material, d is the thickness of the pellet and A is the area of cross-section. ϵ_r and ϵ_0 are the dielectric constant and permittivity of free space respectively [26, 27].

The variation of dielectric constant with frequency of iron doped mullite composites are shown in Fig. 3. From the plot it is clear that in all the cases, dielectric constant decreased with increase in frequency and attained a saturation tendency at 1.5 MHz for a each concentration of doped metal. This behavior of a dielectric may be explained qualitatively by the supposition that the mechanism of the polarization process in mullite-iron nanocomposite is similar to that the conduction process. The electron-hopping model of Heikes and Johnston [28] can explain the electrical conduction mechanism. It is known that the effect of polarization is to reduce the field inside the medium. Therefore, the dielectric constant of a substance may decrease substantially as the frequency is increased [29]. The electronic polarizations can orient themselves with the electric field at the lower frequency range but at higher frequency, the internal individual dipoles contributing to the dielectric constant can't move instantly. So as frequency of an applied voltage increases, the dipole response is limited and the dielectric constant diminishes [30, 31].

The dielectric loss tanδ of each sample was measured in the frequency range 500 Hz to 1.5 MHz and is graphically shown in Fig. 4. It was found that for all samples, tanδ decreases with increasing frequency and reaches constant value at 1.5 MHz.

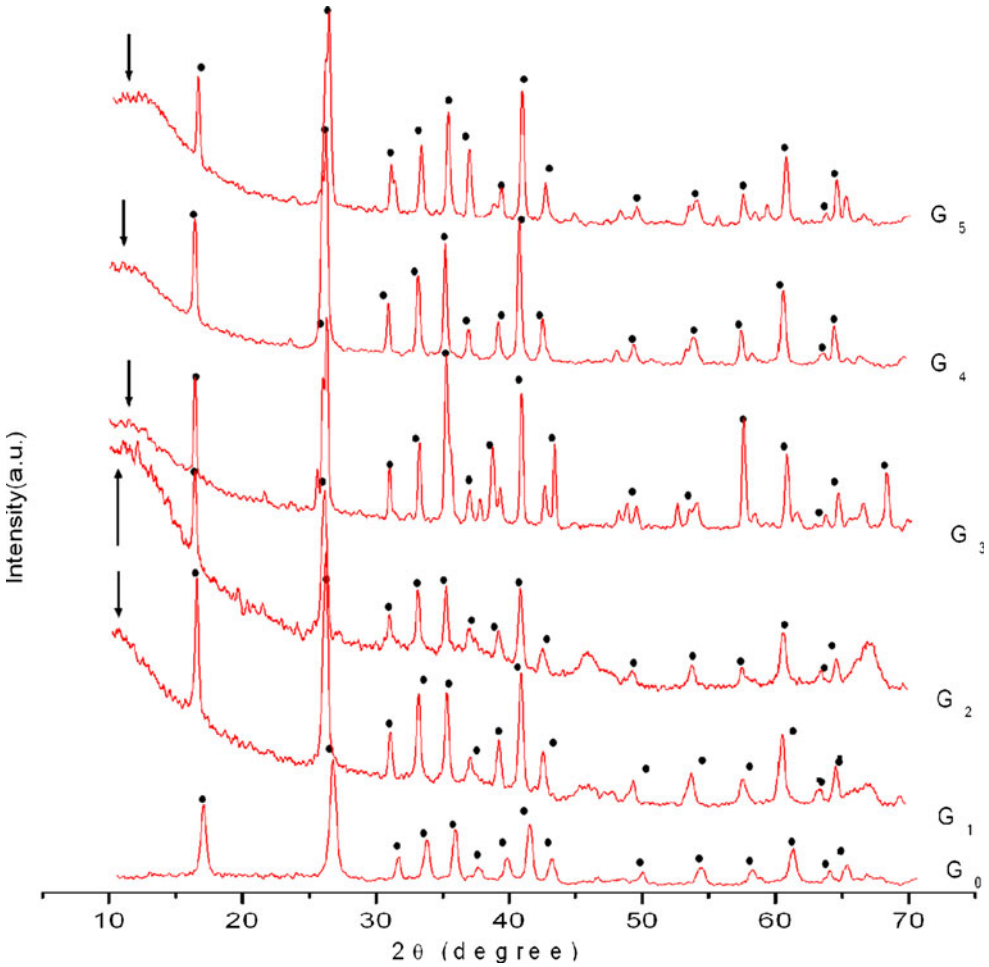

Fig. 1 X-ray diffraction pattern of mullite precursor gels sintered at 1000°C containing increasing concentration of iron (glass phase is indicated by ↓)

A.C. conductivity of the samples were then calculated using the formula

$$\sigma_{a.c.} = 2nf\,tan\delta\,\epsilon_r\,\epsilon_o\,,$$

where f is the frequency in Hz, tanδ is the dielectric loss factor, ϵ_r and ϵo are the dielectric constant of the material and permittivity of free space respectively [27, 32].

In ln $\sigma_{a.c.}$ Vs ln f graph a linear increment of a.c. conductivity with frequency for all doping concentrations is

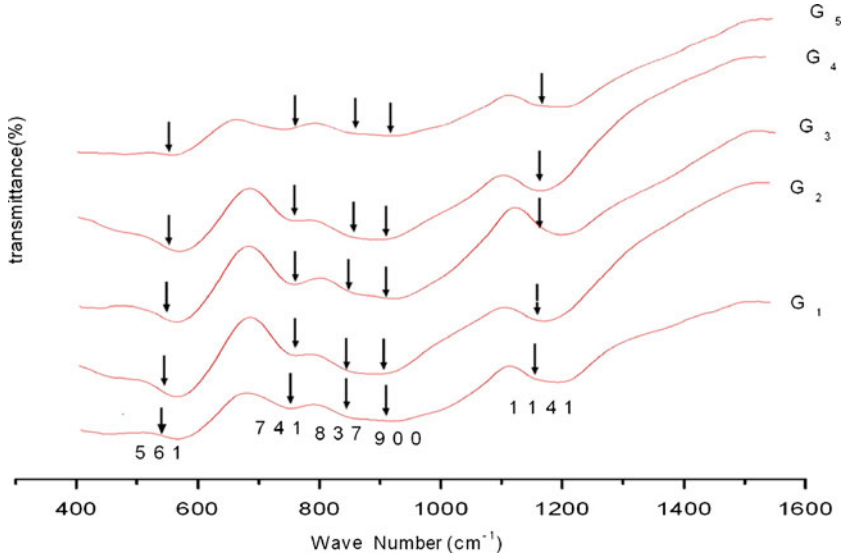

Fig. 2 FTIR micrograph of sample G_1, G2, G3, G4&G_5 sintered gels at 1000°C for 3 hrs.for iron ions

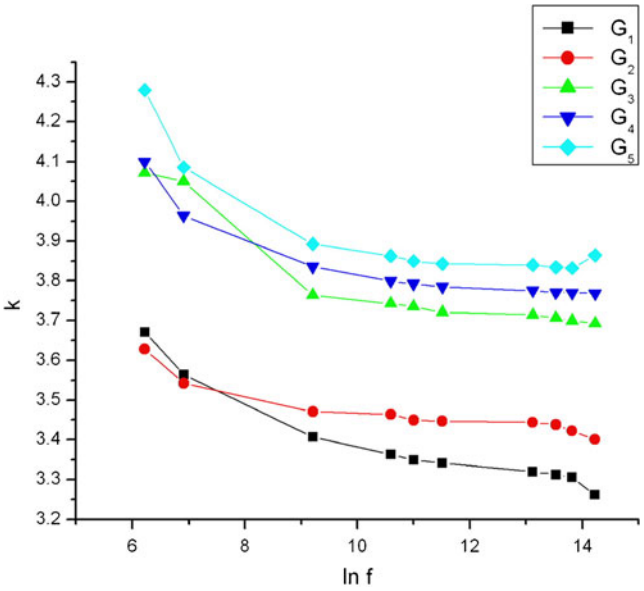

Fig. 3 Variation of dielectric constant with frequency of mullite precursor gels sintered at 1000°C containing increasing concentration iron

observed (Fig. 5).It has been observed that the increment of a.c. conductivity suddenly jumps from G_4 to G_5 .The linearity of the plots follows the frequency dependent part of Jonscher's universal power law which can be represented by the equation

$$\sigma(\omega) = \sigma_{dc} + \sigma_0 \omega^S,$$

Where σ_{dc} is the dc (or frequency independent) conductivity, $\boldsymbol{\sigma_0}$ is a temperature dependent parameter and s lies in the

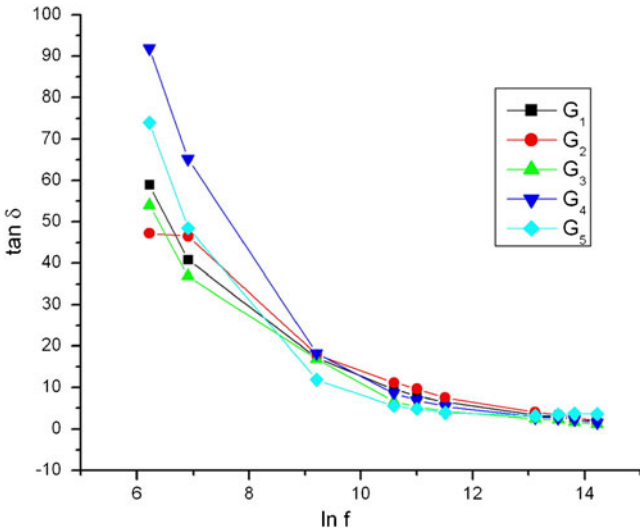

Fig. 4 Variation of dielectric tangent loss with frequency of mullite precursor gels sintered at 1000°C containing increasing concentration iron

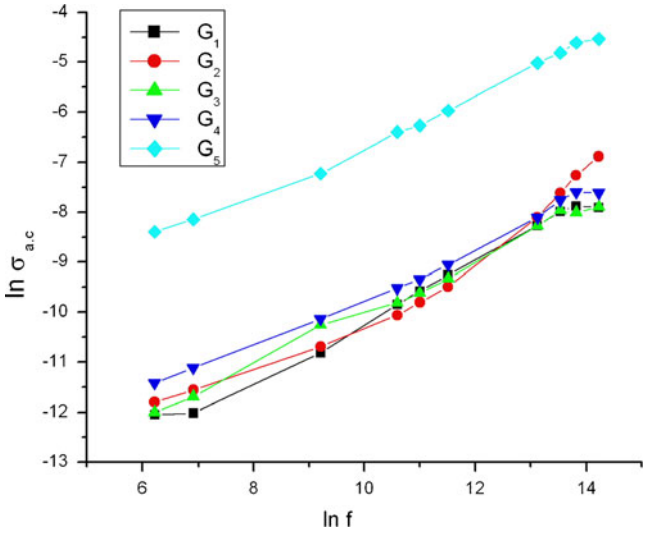

Fig. 5 Variation of a.c. conductivity with frequency of mullite precursor gels sintered at 1000°C containing increasing concentration iron

range $0<s<1$ [32–35]. The linear increase in $\sigma_{a.c.}$ is due to the glassy phase in the sintered gels which increases with the increase of concentration of doped metal (Fig. 1). When there is a large amount of glassy phase present in the structure the mobile ions such as Fe^{3+} and Al^{3+} finds an easy path to move and hence increases the conductivity. Thus, both amount of glassy phase and the concentration of metal ions present in the glassy phase contribute in increasing $\sigma_{a.c}$ of the sintered gels at 1000°C [36, 37].

2.4.5 FESEM

The morphology of the mullite particles of lowest (G_1) and highest (G_5) concentration of the doped metal were investigated by FESEM. The micrograph for G_1 shows almost round shaped particles of mullite of average size 200 nm. Numerous smaller particles can also be seen along with amorphous aggregates [13, 38] (Fig. 6 (a)).

G_5 samples shows distinct elongated morphology of mullite particles of size 350 nm embedded in the matrix (Fig. 6 (b)). The mullite content and crystallization in all the G_5 samples were greater than in G_1 composites indicating the catalytic effect of the metal ions at 1000°C [13, 14].

2.4.6 Magnetic measurements

Over the solubility limit, the iron ions are aggregated-forming particles with a magnetic order that are responsible for the hysteresis loops and observed in G_3, G_4 and G_5 [39–41] (Fig. 7 (a, b, c)). The saturation magnetization is 0.225 T and starts around 260 KA/m (Fig. 7 (c)) for 0.20 M. The narrow hysteresis loop (Fig. 7 (a, b, c)) might suggest a

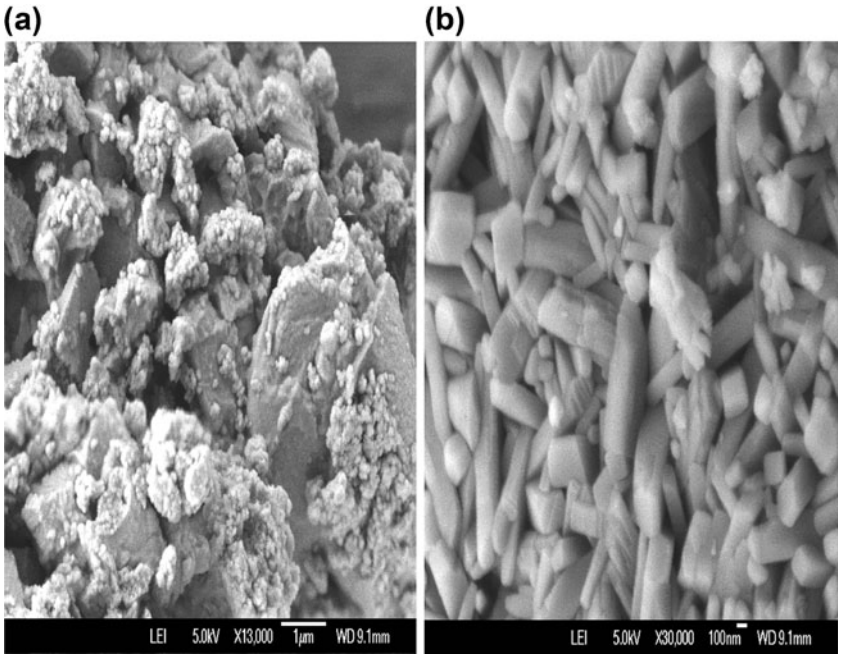

Fig. 6 (**a**, **b**) FESEM of mullite precursor gels doped with Fe for sample G_1 and G_5 sintered at 1000°C

nearly superparamagnetic behaviour of the nanocomposite particles [42].

3 Conclusion

Iron doped mullite composites have been synthesized by sol–gel technique and their phase evolution and dielectric properties have been investigated. The results showed an increase in mullite phase up to G_5 and glassy phase continued to increase with doping concentration. The dielectric constant decreased with frequency for all the samples attaining constancy at high frequency, which is normal behaviour for dielectric ceramics. At 1.5 MHz, G_1 mullite composite gave k value of 3.26. A.c. conductivity increased with frequency following Jonscher's power law and was found to depend on the amount of glassy phase and concentration of mobile ions present in the composites. These composites thus having good dielectric properties at high frequency may be suitable for use as electronic substrates.

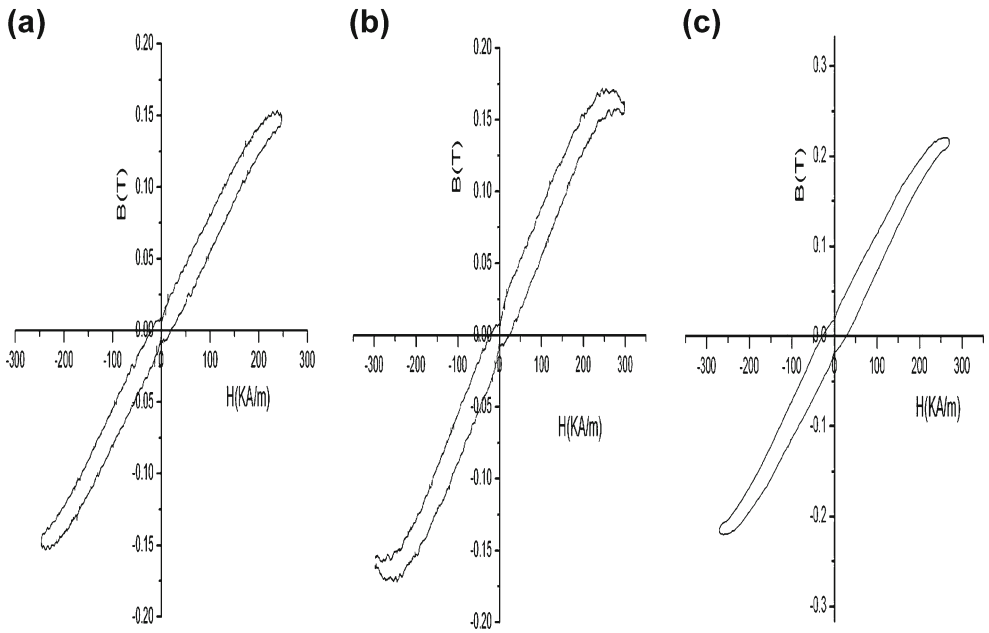

Fig. 7 (**a, b, c**) Hysteresis loop for mullite precursor gels doped with Fe for sample G_3 , G_4 and G_5 sintered at 1000°C

Acknowledgement We are grateful to DST and UGC (PURSE program), Government of India, for the financial assistance and thanks to Mr. Soumyaditya Sutradhar for his help in magnetic measurement.

References

1. K. Maex, M.R. Baklanov, D. Shamiryan, F. Lacopi, S.H. Brongersma, Z.S. Yanovitskaya, Appl. Phys. **93**, 8793–8841 (2003)
2. T. Ebadzadeh, W.E. Lee, J. Eur. Ceram. Soc. **18**, 837–838 (1998)
3. T. Kurihara, M. Horiuchi, Y. Takeuchi, Shin-ichi Wakabayashi, Mullite ceramic substrate for thin film application (Research and Development Department, Shinko Electric Industries Co.Ltd, Nagano City, 381, Japan). **1**, 68–75 (1990)
4. V. Ramakrishnan, E. Goo, J.M. Roldan, E.M. Giess, J. Mater. Sci. **27**, 6127–6130 (1992)
5. V. Viswabaskaran, F.D. Gnanama, M. Balasubramanian, Appl. Clay Sci. **25**, 29–35 (2004)
6. M.A. Camerucci, G. Urretavizcaya, M.S. Castro, A.L. Cavalieri, J. Eur. Ceram. Soc **21**, 2917–2923 (2001)
7. B. Kanka, H. Schneider, J. Mater. Sci. **29**, 1239–1249 (1994)
8. T. Martisius, R. Giraitis, J. Mater. Chem. **13**, 121–124 (2002)
9. A. Esharghawi, C. Penot, F. Nardou, J. Eur. Ceram. Soc. **29**, 31–38 (2009)
10. M. Imose, Y. Takano, M. Yoshinaka, K.O. Hirota Yamaguchi, J. Am. Ceram. Soc. **81**, 1537–1540 (1998)
11. R. Torecillas, S. Aza, S.J. Moya, T. Epicier, G. Fantozzi, J. Mat. Sci. Lett. **9**, 1400–1402 (1990)
12. B.L. Kong, S.T. Zhang, J. Ma, F. Boey, J. Alloys Compd. **359**, 292–299 (2003)
13. B. Bagchi, S. Das, A. Bhattacharya, R. Basu, P. Nandy, J. Am. Ceram. Soc. **92**, 748–751 (2009)
14. B. Bagchi, S. Das, A. Bhattacharya, R. Basu, P. Nandy, J. Sol–gel Sci. Technol. **55**, 135–141 (2010)
15. H. Wang, W.M. Wang, Z.Y. Fu, T. Sekino, K. Niihara, J. Electroceram. **21**, 353–356 (2008)
16. F.J. Berry, R.L. Bilsborrow, A.J. Dent, M. Mortimer, C.B. Ponton, B.J. Purser, K.R. Whittle, Polyhedron. **18**, 1083–1087 (1999)
17. K.C. Song, Mater. Lett. **35**, 290–296 (1998)
18. D. Hoffman, R. Roy, S. Komarneni, J. Am. Ceram. Soc. **69**, 468–471 (1984)
19. M.G. Ferreira da Silva, J. Sol–gel Sci. Technol. **13**, 987–990 (1998)
20. A.K. Chakraborty, J. Mater. Sci. **29**, 6131–6138 (1994)
21. A.K. Chakraborty, J. Mater. Sci. **29**, 1558–1568 (1994)
22. Z. Yingchun, W. Zeshuang, W. Shuming, W. Xiujuan, L. Yanhong, Adv. Mater. Res **177**, 310–321 (2011)
23. R.L. Ore'fice, W.L. Vasconselos, J. Sol–Gel Sci. Technol. **9**, 239–249 (1997)
24. A. Beran, D. Voll, H. Schneider, J. Eur. Ceram. Soc. **21**, 2479–2485 (2001)
25. L.S. Cividanes, T.M.B. Campos, L.A. Rodrigues, D.D. Brunelli, G.P. Thim, J. Sol–gel Sci. Technol. **55**, 111–125 (2010)
26. D.R. Patil, S.A. Lokare, R.S. Devan, S.S. Chougule, C.M. Kanamadi, Y.D. Kolekar, B.K. Chougule, Mater. Chem. Phys. **104**, 254–257 (2007)
27. A. See, J. Hassan, M. Hashim, W. Mohd. Daud Wan Yusoff, Solid State Sci. Tech. **16**, 197–204 (2008)
28. R.R. Heikes, D. Johnston, J. Chem. Phys. **26**, 582–588 (1957)
29. S.F. Mansou, Egypt. J. Solids. **28**, 263–267 (2005)
30. C. Venkataraju, G. Sathiskumar, K. Sivakumar, J. Alloys Compd. **498**, 203–206 (2010)
31. D. Ravinder, G. Ranga Mohan, Prankishan, Nitendarkishan, D.R. Sagar, Mater. Lett. **44**, 256–260 (2000)
32. S. Sindhu, M.R. Anantharaman, B.P. Thampi, K.A. Malini, P. Kurian, Bull. Mater. Sci. **25**, 599–606 (2002)
33. A.R. Kulkarni, P. Lunkenheimer, A. Loidl, Mater. Chem. Phys. **63**, 93–97 (2000)
34. M. Goswami, S.K. Deshpande, R. Kumar, G.P. Kothiyal, J. Phys. Chem. Solids. **71**, 739–744 (2010)
35. F.A. Abdel Wahab, M. Abdel-Baki, J. Non-Crystalline Solids. **355**, 2239–2249 (2009)
36. R.A. Islam, Y.C. Chan, Md.F. Islam, Mater. Sci. Eng. B. **106**, 132–140 (2004)
37. H. Zipkin, L. Israel, S. Guler, C. Guler, Ceram. Inter. **33**, 663–667 (2007)
38. R. Baranwal, M.P. Villar, R. Garcia, R.M. Laine, J. Am. Ceram. Soc. **84**, 951–957 (2001)
39. H. Wang, L. Gao, W. Wang, Z. Fu, T. Sekino, S.W. Lee, J. Cer. Soc. Japan **117**, 452–460 (2009)
40. M.P. Morales, T.G. Carreno, M. Ocana, M. Alonso-Sanudo, C.J. Serna, J. Solid State Chem. **155**, 458–464 (2000)
41. K.J.D. Mackenzie, T. Dougherty, J. Barrel, J. Eur. Ceram. Soc. **28**, 499–502 (2008)
42. E. Vanea, M. Tamasan, C. Albon, V. Simon, J. Non-Crystalline Solid **357**, 3791–3796 (2011)